Tailored Alkene Oligomerization with H-ZSM-57 Zeolite**

Johan A. Martens,* Raman Ravishankar, Igor E. Mishin, and Pierre A. Jacobs

Oligomerization reactions of short alkenes are used in the chemical industry to synthesize speciality C_6-C_{12} alkenes as intermediates for plasticizer and surfactant alcohol synthesis through hydroformylation.[1] Industrial alkene oligomerization processes in the liquid phase produce linear 1-alkenes with transition metal complexes as catalysts.[1–3] To produce branched higher alkenes, the starting alkenes in the liquid, vapor, mixed liquid–vapor, or supercritical phase are treated with heterogeneous acid catalysts.[1, 4, 5]

The phosphoric acid on kieselguhr catalyst, developed in 1935 by Ipatieff and Egloff,[6] is applied for the oligomerization of dilute propene or butene streams at temperatures and pressures up to 520 K and 8.5 MPa, respectively.[7] The catalyst is not selective and the operation conditions are critical. Acidic zeolites and, especially, H-ZSM-5 can be used for converting light alkenes into hydrocarbon fuels and lubricants.[8] Reaction temperatures exceeding 473 K are required to prevent blocking of the channels by deposition of heavy oligomers.[9] In ZSM-5, the oligomer chains undergo linearization before they can diffuse out of the channels.[10] Besides oligomerization, the H-ZSM-5 zeolite catalyzes cyclization and hydrogen transfer reactions leading to complex product mixtures including arenes, cycloalkanes, and alkanes.[11]

Acid-catalyzed alkene oligomerization can be rationalized with alkylcarbenium ion chemistry. The elementary reaction steps comprise 1) protonation of an alkene and formation of an alkylcarbenium ion, 2) addition of a second alkene to the alkylcarbenium ion, 3) eventual skeletal isomerization, and 4) deprotonation. When the approach of the positively charged carbon by the double bond in step 2) is hindered, an allylic hydrogen is transferred, leading to the formation of an alkane and an allylic cation. The latter is a coke precursor.[12] The ideal zeolite catalyst should favor a crosswise arrangement of the alkene and the alkylcarbenium ion to suppress hydrogen transfer (Figure 1).

In the search among the known zeolite structures[13] for suitable pore structures we discovered the ZSM-57 zeolite (MFS topology). It is a less studied zeolite,[14, 15] in which 10-ring pores that run along the crystallographic *a* direction are provided with short wide lobes arising from the partial intersection with 8-ring pores that run along the crystallographic *b* direction (Figure 2). The elliptic 8-rings with

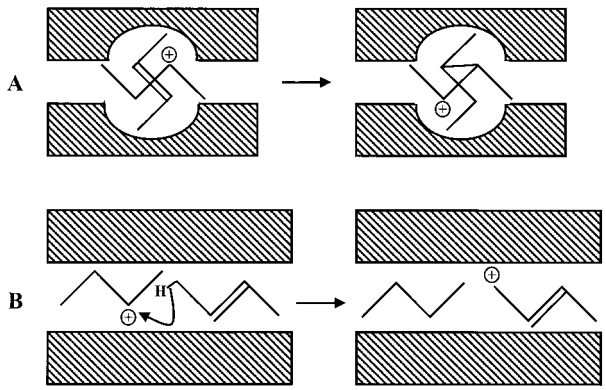

Figure 1. A) Crosswise arrangement of *trans*-but-2-ene and the 2-butyl cation in a lobed pore favoring addition; B) lining up of the molecules in a tubular pore leading to allylic hydride transfer.

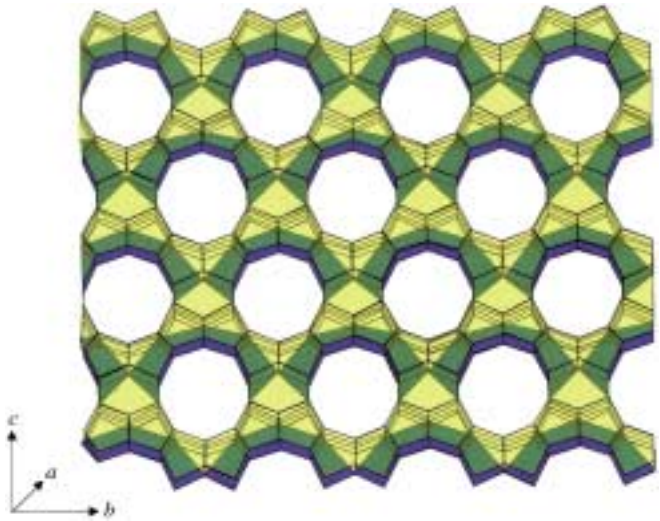

Figure 2. Representation of the MFS framework topology. The lobes along the 10-ring pores are colored in blue.

crystallographic free diameters of 0.33×0.48 nm terminating the lobes are impermeable by hydrocarbons. Two *trans*-but-2-ene molecules were docked in a ZSM-57 cluster and position-optimized with respect to their van der Waals interaction (Figure 3). The channel and lobe structure imposed the desirable crosswise arrangement of the two C_4 chains and favored the resulting formation of the dimer, *trans*-3,4-dimethylhex-2-ene (Figure 3).

ZSM-57 zeolite was synthesized by using *N*,*N*,*N*,*N*′,*N*′,*N*′-hexaethylpentamethylenediammonium ions as template.[16] Molecular models reveal that during the crystallization process, these organic cations are trapped in the channels with their positively charged nitrogen atoms in front of the lobes and impose positioning of balancing framework charges and, after calcination, of acid sites in the lobes. For comparison purposes, zeolite samples representative of the alternative pore types were selected: 10-ring channels without intersections (TON, ZSM-48, AEL topologies), 10-ring channels intersecting with 8-ring channels (FER topology), intersecting 10-ring channels (MFI, MEL), 10- and 12-ring channels without intersections (MWW topology), and intersecting 12-ring channels (BEA* topology). In the experimen-

[*] Prof. J. A. Martens, Dr. R. Ravishankar, Dr. I. E. Mishin, Prof. P. A. Jacobs
Centrum voor Oppervlaktechemie en Katalyse
Katholieke Universiteit Leuven
Kardinaal Mercierlaan 92, 3001 Heverlee (Belgium)
Fax: (+32) 16-321998
E-mail: johan.martens@agr.kuleuven.ac.be

[**] J.A.M. and P.A.J. acknowledge the Flemish government for a research grant (G.O.A.).

  1433-7851/00/3923-4376 $ 17.50+.50/0

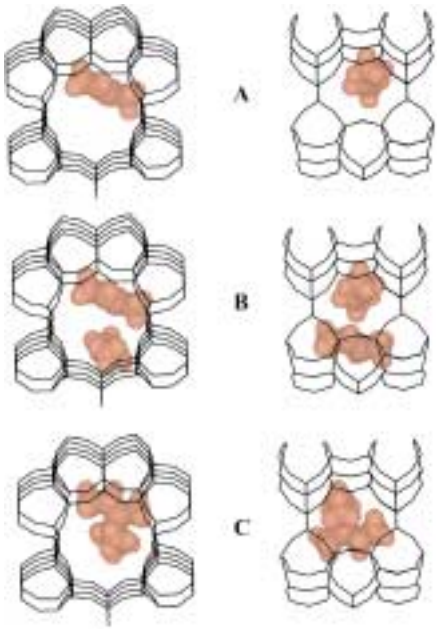

Figure 3. Crosswise arrangement of *trans*-but-2-ene molecules in the ZSM-57 pores giving rise to the formation *trans*-3,4-dimethylhex-2-ene (view along the 10-ring channels (left) and of the 8-ring channels (right) of the zeolite). A) A single *trans*-but-2-ene molecule preferentially adsorbed in the lobe; B) second *trans*-but-2-ene molecule positioned in the channel; C) position-optimized *trans*-3,4-dimethylhex-2-ene molecule retaining the perpendicular orientation of the original C_4 molecules.

tal evaluation of the but-2-ene oligomerization activity of these catalysts (Table 1), the reaction temperature was increased stepwise starting at 353 K until the but-2-ene conversion exceeded 60 %. With all catalysts, double-bond shift was rapid and thus in the expression of conversion, all C_4 double-bond isomers were lumped and considered as unconverted feed.

The H-ZSM-57 catalyst gave a high butene conversion of 89 % at 353 K. With the other zeolites, higher temperatures of 383 – 483 K were necessary to achieve similar conversions (Table 1). H-ZSM-57 combined high activity with high selectivity for C_8 alkenes (86 %). C_{12} alkenes were formed in minor amounts. Other catalysts were substantially less selective for C_8.

H-ZSM-57 was active even at 298 K. The but-2-ene conversion of 33 % after 1 h dropped below 1 % in the second hour on stream at this temperature. At 353 K, the but-2-ene conversion decreased more slowly with time on-stream. After conversion of about 20 g butene per gram of zeolite, the butene conversion was still 60 % with a C_8 selectivity of 91 %. An increase in temperature of 20 K restored the initial activity and led to still slower decay with time on-stream. The temperature was increased stepwise to 473 K to balance deactivation with preservation of the high C_8 selectivity. Cracking and other side reactions started occurring only at temperatures exceeding 473 K. H-ZSM-57 zeolite can be periodically regenerated by calcination in air.

The expected primary products from the acid-catalyzed condensation of two but-2-ene molecules and of but-1-ene with but-2-ene are 3,4-dimethylhexenes and 3-methylheptenes, respectively. At 298 K, these products represented 76 and 9 % of the C_8 product fraction, respectively. The other products were isomers in which methyl groups had shifted. At higher reaction temperatures, methyl shifts were more important. Branching and de-branching of C_8 products were limited. At 423 K, the C_8 fraction contained only 2.8 % linear octenes and 1.4 % tribranched octenes.

Molecular modeling and repulsion energy calculations[17] (Table 2) were useful for rationalizing the oligomerization behavior of H-ZSM-57. Propene, *n*-butene, and *n*-pentene molecules fit in the lobe and leave enough free space in the channel for reaction with any linear or methyl-branched alkene. Isobutene can dimerize and codimerize with isopentenes, but reaction with heavier methyl-branched alkenes is sterically hindered. *n*-Hexenes, methylpentenes, and methylhexenes are repulsed from the lobe. When adsorbed in the channel, they can be combined with C_3, *n*-C_4, or *n*-C_5 alkenes in the lobe. Among the dimethyl-branched alkenes, the

Table 2. Excess repulsion potential [kJ mol^{-1}] of alkenes in ZSM-57.[a]

Alkene in channel	Alkene in lobe							
	n-C_3	*n*-C_4	*i*-C_4	*n*-C_5	*i*-C_5	*n*-C_6	MB-C_6	MB-C_7
C_3	0	0	0	0	1	13	11	25
n-C_4	0	2	0	0	2	11	6	24
i-C_4	0	1	0	0	0	12	23	51
n-C_5	0	1	7	0	3	38	12	51
i-C_5	0	2	8	1	27	16	23	27
n-C_6	0	2	0	2	2	35	12	100
MB-C_6	0	3	11	2	28	16	44	n.d.
n-C_7	0	2	7	2	2	9	29	n.d.
MB-C_7	5	5	85	14	28	41	n.d.	n.d.
DB-C_8[a]	31	n.d.	n.d.	n.d.	n.d.	n.d.	n.d.	n.d.

[a] MB and DB: monomethyl-branched and dimethyl-branched isomers, respectively; n.d. = not determined.

Table 1. Screening of the zeolite catalyst for the oligomerization of 2-butene.[a]

Zeolite	Topology code	Si/Al	*T* [K]	Conversion [%]	Product distribution [wt %]				
					$C_6 - C_7$	C_8	$C_9 - C_{11}$	C_{12}	C_{13}[b]
H-ZSM-57	MFS	27	353	89	0.3	85.7	1.1	12.8	0.0
H-ZSM-48	–	50	383	82	0.9	60.5	9.9	24.9	3.8
H-Beta	BEA*	12.5	393	79	1.2	50.7	14.1	28.9	5.0
H-Ferrierite	FER	6.2	413	66	1.5	69.5	7.6	19.8	1.6
H-SAPO-11	AEL	–	413	73	1.4	60.7	7.7	24.8	5.5
H-ZSM-11	MEL	45	413	90	2.3	56.6	10.8	26.8	3.6
H-ZSM-22	TON	30	423	82	0.9	57.6	4.0	30.4	7.2
H-MCM-22	MWW	45	433	95	6.1	52.2	22.2	19.5	0.0
H-ZSM-5	MFI	26	435	72	5.9	56.8	13.9	23.4	0.0

[a] Feed composition: 2-butene (16 wt %); propane (78 wt %); pentane (6 wt %), *W*/*Fo*: 115 kg s mol^{-1}. [b] C_{13} and higher oligomers.

  1433-7851/00/3923-4377 $ 17.50+.50/0

dimethylpentenes undergo least repulsion when combined with propene in the lobe. Severe repulsion is encountered with dimethylhexenes in the channel in combination with any alkene in the lobe.

The experimentally observed low formation of C_{12} alkenes from C_4 alkenes on H-ZSM-57 (Table 1) is explained by the low reactivity of the C_8 fraction which mainly comprises dimethylhexenes. The C_{12} products were dibranched or tribranched, confirming their formation out of linear or monobranched C_8 isomers, respectively.

In an experiment with pent-1-ene at 373 K and at a pentene conversion of 60%, dimethyl-branched C_{10} alkenes were selectively formed. The subsequent formation of C_{15} alkenes by reaction of pentenes with dimethyl-branched isodecenes was suppressed, as expected.

Other experiments were concerned with a $C_3 + C_4$ mixture (Figure 4). Propene and butene were equally reactive. The primary products were $C_6 - C_9$ alkenes originating from dimerization and codimerization of C_3 and C_4 alkenes and

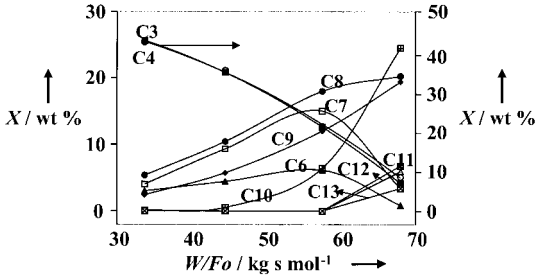

Figure 4. Distribution X [wt%] of the reaction products of a propene–butene mixture converted in the supercritical phase on H-ZSM-57 at different contact times W/Fo [kg s mol^{-1}] at 423 K (W = catalyst weight; Fo = molar flow rate of alkenes at reactor inlet. The feed composition is given in Table 1.

codimerization of methylpentenes and C_3 alkenes, all favored in the lobe and channel system (Table 2). At long contact times, the monomethyl-branched C_6 isomer and the monomethyl- and dimethyl-branched C_7 alkenes reacted further to give $C_8 - C_{13}$ alkenes. These molecules with two or more methyl branchings cannot be properly coadsorbed with any of the shorter molecules and are inert to this catalyst.

In binary $C_3 + C_5$ and $C_4 + C_5$ mixtures, the two alkenes were also equally reactive (Table 3). The products had carbon numbers from C_6 up to C_{13}, peaking at $C_8 - C_{11}$. The main products from the $C_3 + C_5$ mixture can be explained by the favored dimerization and trimerization of C_3 alkenes, codimerization of C_3 and C_5 alkenes, and dimerization of C_5 alkenes. Alternative condensations occurred less, since they involve less appropriate molecule combinations. The mixture of $C_4 + C_5$ leads to C_8, C_9, and C_{10} alkenes through favored dimerizations and codimerizations. The less significant formation of C_{12} and C_{13} products is explained by condensations of methyl-branched C_8 isomers with C_4 and C_5 alkenes, respectively.

In all these experiments, the saturation selectivity of the feed alkenes into the corresponding alkanes was below 0.8%. With other zeolites, the selectivity for double-bond saturation

Table 3. Conversion and distrbution of products in the oligomerization of binary alkene mixtures over H-ZSM-57 at 423 K.

	$C_3 + C_4$[a]	$C_3 + C_5$[b]	$C_4 + C_5$[c]
		Conversion [%]	
C_3	86	93	–
C_4	83	–	90
C_5	–	85	87
		Product distribution [wt%]	
C_6	1	5	0
C_7	4	0	0
C_8	24	41	9
C_9	23	22	36
C_{10}	29	10	37
C_{11}	8	18	0
C_{12}	7	6	12
C_{13}	4	0	5

[a] Feed composition: propene (7 wt%), 1-butene (7 wt%), isobutane (76 wt%), pentane (5 wt%); W/Fo: 68 kg s mol^{-1}. [b] Feed composition: propene (9.8 wt%), 1-pentene (8.9 wt%), butane (74.5 wt%), isobutane (6.8 wt%); W/Fo = 72 kg s mol^{-1}. [c] Feed composition: 1-butene (7 wt%), 1-pentene (10 wt%), propane (10 wt%), isobutane (76 wt%); W/Fo: 158 kg s mol^{-1}.

was substantially higher, for example, around 10% with H-ZSM-22 (Table 1).

The exceptional activity, stability, and selectivity of H-ZSM-57 in alkene oligomerizations is the result of the lobate–pore structure, which favors a crosswise arrangement of alkenes and thus suppresses hydride transfer. With H-ZSM-57, the molecular weight of the oligomers can be tailored by mixing the appropriate short alkenes.

Experimental Section

Catalytic experiments were performed in a fixed-bed down-flow reactor filled with zeolite powder compressed into particles with diameters of 250–500 μm. The dead volume in the reactor tube was filled with glass beads of similar diameters. The feedstocks were prepared by mixing pure compounds in a storage vessel equipped with magnetic stirrer and pressurized at 7 MPa. The liquid feedstock was delivered to the reactor by means of an electronic mass flow controller for liquids. The pressure in the reactor was kept at 6 MPa. Product samples taken at the reactor outlet with a sampling valve with internal volume of 0.1 μL were analyzed on-line by gas chromatography. The skeletal branching and carbon number of the oligomers were analyzed off-line by gas chromatography with a catalytic hydrogenation module.

For the evaluation of the Lennard-Jones (12-6) interaction potential of an alkene and H-ZSM-57 zeolite, a rigid and purely siliceous MFS framework was considered. Dispersion and repulsion constants were taken from reference [17]. All calculations were done on a framework fragment of 1280 oxygen atoms. The geometry of the organic molecule was optimized by using Hyperchem software from Hypercube Inc. This geometry-optimized molecule was introduced into the lattice fragment, and its position optimized following a translation–rotation steepest descent procedure in three dimensions. The excess repulsion potential (Table 2) is the difference between the potential energy of the considered alkene and that of a position-optimized monomethyl-branched alkene of the same molecular weight. These potentials are -79, -91, -107, -120, -133, -144, -154, and -164 kJ mol^{-1} for C_6 to C_{13} isomers, respectively.

Received: June 19, 2000 [Z15285]

[1] K. Weissermel, H.-J. Arpe, *Industrial Organic Chemistry*, VCH, Weinheim, **1993**.
[2] F. Nierlich, *Hydrocarbon Process.* **1992**, *2*, 45–46.
[3] Y. Chauvin, J. Gaillard, J. Léonard, P. Bonnifay, J. W. Andrews, *Hydrocarbon Process.* **1982**, 110–112.

  1433-7851/00/3923-4378 $ 17.50+.50/0

[4] R. L. Shubkin, *Synthetic Lubricants and High-Performance Functional Fluids* (Ed.: R. L. Shubkin), Marcel Dekker, New York, **1993**, pp. 1 – 40.
[5] C. T. O'Connor, M. Kojima, *Catal. Today* **1990**, *6*, 329 – 349.
[6] V. N. Ipatieff, B. B. Corson, G. Egloff, *Ind. Eng. Chem.* **1935**, *27*, 1077 – 1081.
[7] S. A. Tabak, F. J. Krambeck, W. E. Garwood, *AIChE J.* **1986**, *32*, 1526 – 1531.
[8] K. G. Wilshier, P. Smart, R. Western, T. Mole, T. Behrsing, *Appl. Catal.* **1987**, *31*, 339 – 359.
[9] J. P. van den Berg, J. P. Wolthuizen, A. D. H. Clague, G. R. Hays, R. Huis, J. H. C. van Hooff, *J. Catal.* **1983**, *80*, 130 – 138.
[10] C. S. H. Chen, R. F. Bridger, *J. Catal.* **1996**, *161*, 687 – 693.
[11] R. J. Quann, L. A. Green, S. A. Tabak, F. J. Krambeck, *Ind. Eng. Chem. Res.* **1988**, *27*, 565 – 570.
[12] C. Naccache, *Deactivation and Poisoning of Catalysts*, *Chemical Industries Series Vol. 20*, Marcel Dekker, New York, **1985**, pp. 185 – 203.
[13] W. M. Meier, D. H. Olson, C. Baerlocher, *Zeolites* **1996**, *17*, 1 – 230.
[14] S. Ernst, J. Weitkamp, *Stud. Surf. Sci. Catal.* **1991**, *65*, 645 – 652.
[15] J. L. Schlenker, J. B. Higgins, E. W. Valyocsik, *Zeolites* **1990**, *10*, 293 – 296.
[16] E. W. Valyocsik, N. M. Page, *Eur. Pat. Appl.* 174121, **1986**.
[17] S. D. Picket, A. K. Nowak, J. M. Thomas, A. K. Cheetham, *Zeolites* **1989**, *9*, 123 – 135.

Tribochemical Activation of Iron Oxide for the Reduction of NO with CO: How Lattice Defects Can Influence the Catalytic Activity

Thomas Rühle, Olaf Timpe, Norbert Pfänder und Robert Schlögl*

The cleavage of NO_x molecule into its constituent elements is an important goal for environmental catalysis.[1] Massive metal oxides are, in principle, a suitable class of compounds[2] and have been discussed for a long time as potential catalysts,[3] however had neither the required activity nor stability against reduction.

Iron oxide is non-toxic and chemisorbs NO very well[4] and is thus a promising material, provided that the active centers can be regenerated by a reducing agent such as CO.[5] Iron oxide nano particles are currently the subject of extensive investigations in NO reduction processes.[6] nonstationary kinetic measurements[7] show that in hematite (α-Fe_2O_3) NO is absorbed and activated at defects in the oxygen sublattice.[8] Conversion into N_2 proceeds via the intermediate N_2O. The active sites are regenerated by the reaction of CO with oxygen. In comparison to other catalysts iron oxide exhibits a high selectivity for N_2, but not for N_2O,[6, 9] an important feature for application in environmental catalysis.

When the reaction with CO is not limited to the surface active sites then the catalysts is rapidly following the chemistry of the blast-furnace reduction of iron oxide. This reaction pathway requires the diffusion of iron out of the bulk material and onto the surface.[10] Thus it is necessary to maximize the number on active sites but at the same time the bulk diffusion of the iron atoms has to be controlled.

The tribochemical (that is, induced through high-energy ball milling) activation of commercial hematite leads to a clear improvement in the catalytic properties of the material. The conversion – temperature profile (Figure 1) shows a considerable increase in catalytic activity after the grinding process. At the temperature at which the unactivated oxide begins to react the activated sample shows its greatest activity. Compared to supported oxide particles[7] that give active catalysts with an internal surface of 302 $m^2 g^{-1}$ the catalyst presented herein, which has an internal surface of only 8.2 $m^2 g^{-1}$, is significantly more active, as can be seen by comparing the measured values at 50 % conversion (here 482 K, supported sample 578 K) and at 80 % conversion (here 532 K, supported sample 615 K). The comparison of the almost identical NO conversion and CO_2 yield curves in Figure 1 demonstrates clearly the excellent selectivity[11] of the catalyst to N_2, that is achieved here even without a high surface-area activated charcoal support and the addition of promoter oxides.[12] This result also demonstrates the high stability of the ground iron oxide against irreversible reduction.

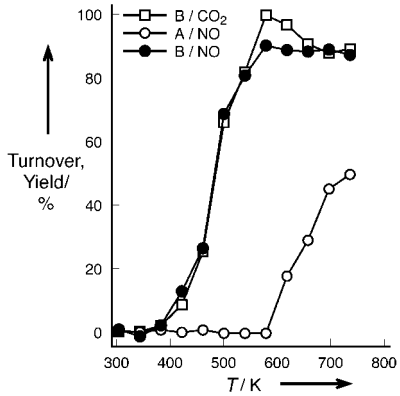

Figure 1. Conversion – temperature profile of the NO – CO reaction on pure unactivated (A) and activated iron oxide (B) (For B/CO_2 it is not the conversion but the yield curve). After activation the Brunauer – Emmett – Teller (BET) surface is not measurably different from the starting value. The modified residence time[7] was in each case 100 kg s mol^{-1}.

The effect of the tribochemical treatment on the activity was emphasized by comparing the activation energies of the NO reduction by iron oxide and by a highly dispersed platinum catalyst[13]. Figure 2 shows the Arrhenius plot of the corresponding data from stationary measurements. The activation improves the specific activity of the iron oxide compared to that of the supported platinum metal. Moreover, the apparent activation energy of the reaction on the iron oxide reduces from 82 to 45 kJ mol^{-1} and is thus comparable to that of the platinum catalyst (50 kJ mol^{-1}; a value that compares well with literature data[14]). This observation is noteworthy because the mechanism of the reactions on platinum and iron ought to be different.[15]

[*] Prof. Dr. R. Schlögl, Dipl.-Chem. T. Rühle, Dr. O. Timpe, N. Pfänder
Fritz-Haber-Institut der Max-Planck Gesellschaft
Faradayweg 4 – 6, 14195 Berlin (Germany)
Fax: (+49) 30-8413-4401
E-mail: andrea@fhi-berlin.mpg.de

  1433-7851/00/3923-4379 $ 17.50+.50/0